ADVANCED MATERIALS INTERFACES
Open Access
www.advmatinterfaces.de

Development and Implementation of Microbial Antifreeze Protein Based Coating for Anti-Icing

Zülal Muganlı, Shaghayegh Saeidiharzand, Regina Rekuviene, Vykintas Samaitis, Audrius Jankauskas, Ali Koşar, Ghazaleh Gharib,* and Abdolali Sadaghiani**

Ice formation on a solid surface is a major challenge in industrial applications, it causes higher energy consumption and performance deterioration and may lead to catastrophic results. The preparation of anti-icing surfaces to prohibit ice accumulation on a surface is crucial to reduce operational costs and to extend the surface's lifetime. The utilization of cryoprotectants to obtain anti-icing surfaces is an effective method and is applicable in multiple fields. Antifreeze proteins (AFPs) are natural cryoprotectants to obtain anti-icing surfaces, which have the ability to decrease the freezing point and to prevent ice-crystal growth via thermal hysteresis (TH) and ice recrystallization inhibition (IRI). This study reports the molecular cloning, expression, and production of AFP protein from *Escherichia coli (E. Coli)*. This wok also demonstrates the activity of coated AFP on aluminum surfaces. The expressed AFP is immobilized on aluminum surfaces treated by oxygen plasma. The coated AFP exhibits promising antifreeze activity with a high anti-icing ability on aluminum surfaces in the size of evaporator fins (40 × 40 cm). The outcome of this study provides new insights into the biotechnological implementation of AFPs to various industrial applications for energy-saving and higher performance.

1. Introduction

Ice accumulation on metallic surfaces is a critical issue that deteriorates industrial outcomes. The added weight caused by ice formation adversely affects wind turbines, aircraft wings, and electrical devices.[1] Ice accretion on condensers of energy systems increases power consumption, whereas ice on roads might result in accidents.[2] Developing substrates having anti-icing properties decreases the ice adhesion strength on a surface while extending the lifetime of the surface by reducing operational costs.[3] To moderate ice accumulation on surfaces used in the industry, both passive anti-icing materials (AIM) (i.e., polyelectrolyte brushes, superhydrophobic surfaces (SHSs), low elastic modulus surfaces) and active de-icing methods (i.e., thermal heating, mechanical removal, chemical fluid spraying) have been employed.[4] Conventional passive AIMs lack mechanical durability and low ice adhesion strength maintenance. In contrast, active de-icing methods have issues with high operational costs and energy demands, environmental pollution, efficiency, and safety deficiencies.[4,5] For instance, the adhesion strength of ice on a smooth surface is much less than on SHSs due to interlocking effects between ice and rough surface, which constitutes an obstacle against applications of SHSs as anti-icing materials.[6] Besides, the widely used active de-icing method, electrothermal heating, might lead to surface overheating in an

Z. Muganlı, S. Saeidiharzand, A. Koşar, G. Gharib, A. Sadaghiani
Faculty of Engineering and Natural Sciences (FENS)
Sabanci University
Orhanli, Istanbul 34956, Turkey
E-mail: kosara@sabanciuniv.edu; ghazalehgharib@sabanciuniv.edu; abdolali@sabanciuniv.edu

Z. Muganlı, S. Saeidiharzand, A. Koşar, G. Gharib, A. Sadaghiani
Sabanci University Nanotechnology and Application Centre (SUNUM)
Sabanci University
Tuzla, Istanbul 34956, Turkey

The ORCID identification number(s) for the author(s) of this article can be found under https://doi.org/10.1002/admi.202300021.

DOI: 10.1002/admi.202300021

R. Rekuviene, V. Samaitis, A. Jankauskas
Ultrasound Research Institute
Kaunas University of Technology
Baršausko St. 59, Kaunas LT-51423, Lithuania

A. Koşar, G. Gharib, A. Sadaghiani
Center of Excellence for Functional Surfaces and Interfaces for Nano-Diagnostics (EFSUN)
Sabanci University
Orhanli, Istanbul 34956, Turkey

G. Gharib
Nordcee
Department of Biology
University of Southern Denmark
Campusvej 55, Odense DK-5230, Denmark

uncertain environment.[7] In addition, several materials such as modification of the surface structure and properties by using nanosilica,[8] polysiloxane-modified carbon nanotubes, fluorine-silicone-resin,[9] and fluorosilane-modified epoxy have been employed to obtain anti-icing surfaces.[10] Nevertheless, most of them consist of labor-intensive processes and high-cost equipment.[11] The use of cryoprotectants is an effective method to acquire anti-icing surfaces, and they have been utilized in various fields such as agriculture, food technology, therapeutics, cosmetics, and industry.[12–14] Among recently used cryoprotectants such as glycols, dimethyl sulfoxide (DMSO), and glycerol, antifreeze proteins (AFPs) have gained a reputation due to their innate ice-binding properties and safety profile.[11,15]

AFPs function as natural cryoprotectants that play a significant role for many organisms, including Antarctic marine fishes, to keep them alive under sub-zero conditions.[16] AFPs are classified as specific types of proteins, peptides, and glycopeptides that can bind to various angles of ice crystals and hamper their growth. They can be isolated from several species, such as microorganisms, plants, arthropods, and fish, with distinctive structures resulting from the origin of the species.[17] AFPs have six categories, namely, AFPs I, AFPs II, AFPs III, AFPs IV, hyperactive AFPs, and anti-freezing glycoprotein AFPs, based on their structural differences.[18] They have the ability to modify the formation of embryonic ice crystals by being attached to particular crystal planes, thereby inhibiting ice growth.[19] The working mechanism of AFPs (while interacting with ice) is based on depressing the water's freezing point with the prevention of ice crystal growth.[20,21] Thermal hysteresis (TH) and ice recrystallization inhibition (IRI) are the two key factors that identify the activity of AFPs.[22] TH can be described as the temperature gap between the melting and freezing points, which indicates the activity of AFPs. TH activity has a crucial role in the freeze avoidance mechanism, which is vital for organisms to inhibit freezing of the body fluids at below 0 °C.[23] Enlargement of ice crystals from the presence of the smaller ones is defined as the ice recrystallization (IR) phenomenon with Kelvin effect.[24] IR consists of ice grain boundary migration, which suggests that small ice crystals vanish whereas large ones increase in size since large ice crystals, have lower free energy, and are thermodynamically more stable.[23,25] AFPs have IRI activity that prevents grain boundary migration by ceasing the growth of ice and melting it at the boundaries. There are many antifreeze glycoproteins to inhibit ice growth, recrystallization, and nucleation. Therefore, several attempts have been made to employ AFPs as cryoprotective agents.[22] Since the formation of ice crystals is challenging for multiple fields, AFPs have been utilized in various areas such as agriculture, anti-icing materials, food industry, and cryomedicine.[23] AFPs are efficient biomaterials for anti-icing applications due to their environmentally friendly profile and natural attachment through ice-crystal planes to inhibit ice-crystal growth with TH and IRI activities. However, these proteins can be easily denatured when exposed to a high temperature, a high salt concentration in the buffer solution, and pH change, and they might lose their stability.[26] Therefore, the parameters leading to AFP denaturation must be well considered to achieve effective and sustainable anti-icing systems. Coatings have been applied in many applications, such as chemistry, agriculture, medicine, automotive, and energy industries. The development of coatings is required to functionalize the materials to obtain specific properties such as anti-freezing, wear resistance, anti-UV property, fire-resistance, anti-corrosion, and antimicrobial property.[27–33] Biomaterial-based surface modification techniques have been utilized to reduce the negative environmental effects of coatings which are utilized to increase energy efficiency, anti-fogging surfaces, and flame-retardant fabrics.[34–37] Among biomaterials, AFPs exhibit anti-icing properties where AFP is used as a coating agent on metallic surfaces and can be utilized in multiple industrial applications.[20] For instance, an anti-icing surface was achieved by the polymer-linked conjugation of AFPs on a glass surface, and a polymer coating enhanced the stability of AFPs on the glass surface.[38] In another study, Gwak et al. reported that AFP-coated aluminum surfaces had low supercooling points. The addition of trehalose delayed the denaturation of AFP by forming hydrogen bonds between hydroxyl groups of trehalose and polar residues in proteins.[11,39] Furthermore, an antifreeze coating for windshields was developed on a glass surface by mixing antifreeze polypeptides and silane coupling agents.[40] Moreover, Jeonn et al. prepared anti-icing surfaces by employing AFPs on PDA-treated aluminum with the use of Tannic acid (TA) coating.[41]

Aluminum is the third most abundant element on the Earth and a highly produced metal after steel.[42,43] It has low density, is nontoxic, has high thermal conductivity, and can be easily cast, machined, and formed. As one of the most recycled commodities, such properties make aluminum eligible for its extensive use in the automotive, electrical distribution, transportation, building, aerospace, and packaging industries.[43] Nevertheless, ice formation leads to severe damage to systems and higher energy consumption where aluminum surfaces with anti-icing properties are essential.[11]

In this study, we performed molecular cloning, expression, and production of AFP protein in *Escherichia coli (E. Coli)* strain Rosetta (DE3) and its coating on Al surfaces. A synthetic AFP gene (pUC-AFP) encoding for afp*A* protein was designed, and the gene was subcloned in the expression vector, pET_{28}.[44] Subsequently, the AFP protein was produced in Rosetta *E. coli* host cells. The recombinant AFP was ionically bonded to Al surfaces by oxygen plasma, and the anti-icing activity was monitored by a lab-made experimental setup. To the best of our knowledge, for the first time, this study demonstrates the recombinant protein technology and immobilization of AFPs on aluminum surfaces using synthetic AFP gene for anti-icing purposes. The outcome of this study provides new insights into the biotechnological implementation of AFPs to various industrial applications with large-scale protein production efficiency.

2. Experimental Section

2.1. Reagents and Chemicals

Chemicals and enzymes used in this study were purchased from Sigma (USA), Merck (Germany), and Fisher Scientific (Leicestershire, UK). Restriction enzymes, DNA markers, T4 DNA ligase, DNA isolation kit, and DNA extraction kits were purchased from Thermo Fisher Scientific (MA, USA),

Taq DNA polymerase from Oligonucleotide primers were been synthesized by Oligomer Company (Ankara, Turkey), and pUC-AFP gene was synthesized by Integrated DNA Technologies (Iowa, USA). Lurian Broth Medium, isopropyl β-d-1-thiogalactopyranoside (IPTG), Trizma Base, Bromophenol Blue, Coomassie Blue Reagent, sodium dodecyl sulphate, ammonium persulfate, 30% polyacrylamide were purchased from Sigma. Tetramethylethylenediamine (TEMED) was purchased from Neofroxx (Germany).

2.2. Construction of AFP Recombinant Cloning and Expression Vector

The cloning construct, pUC-AFP that encodes the afpA protein in Mryoi et al. first was chemically transformed in *E. coli* DH5α.[44,45] The formed plasmid constructs were isolated by GeneJet Plasmid Miniprep kit. The isolated constructs were restricted by Nde I (5″-CATATG-3″) and Xho I (5″-CTCGAG-3″) restriction enzymes. The size of the isolated and restricted constructs was evaluated by agarose gel electrophoresis, and their concentrations were obtained by Nanodrop (Thermo Scientific 2000c). The amplified AFP gene was subcloned to the expression vector, pET_{28}, which contains a nickel his-tag. The generated construct, pET_{28}-AFP, was isolated, and its size was evaluated by agarose gel electrophoresis. Sequencing analysis of recombinant pET_{28}-AFP was conducted by BM Labosis company. For this purpose, bidirectional sanger sequencing was utilized using Universal T7 primers. Herein, bidirectional sequencing refers to the sequencing of an initial fragment of DNA from its top and bottom strands, where the top and bottom sequence reads can be matched and compared.[46] After the sequence confirmation, the pET_{28}-AFP was transformed into *E. coli* strain Rosetta (DE3). The expressed product was analyzed by sodium dodecyl sulphate-polyacrylamide gel electrophoresis (SDS-PAGE). **Figure 1**a displays the procedure of the recombinant AFP production.

2.3. Production Optimization, IPTG Induction, and Purification of AFP

Protein production was made by inoculation of Rosetta-pET_{28}-AFP overnight at 37 °C, 200 rpm. A total of 1% of the growth was transferred to 5 mL LB medium and was incubated at a shaker incubator until the OD (600 nm) reached 0.4 abs. When OD reached 0.4 abs, 0.5×10^{-3} M IPTG induction was done, and the induced cell suspension was incubated at 30 °C for 4 h. After induction, the cell suspension was centrifugated at 8000 rpm, 4 °C for 10 min. The remaining pellet was dissolved in Tris-Cl buffer (pH 8) to stabilize the protein content. The recombinant AFP protein production was optimized using several parameters such as induction time (4 h and 24 h), IPTG concentration (0.5×10^{-3}, 0.8×10^{-3}, and 1×10^{-3} M), induction temperature

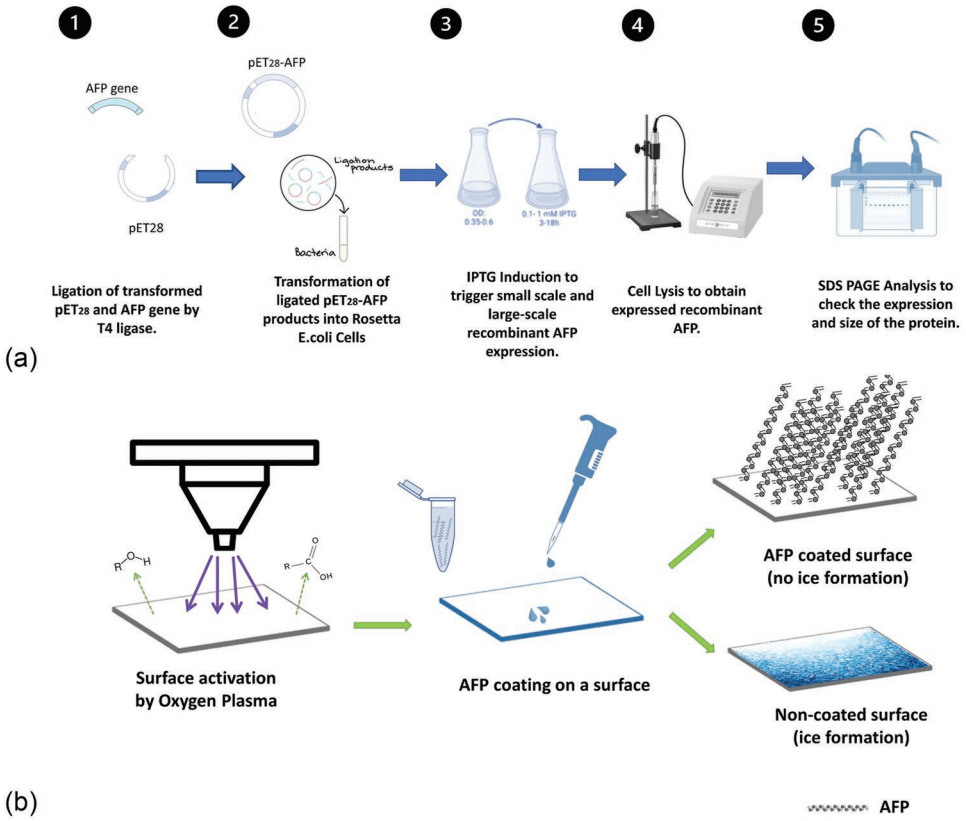

Figure 1. a) Schematic of the basic methodology of the recombinant cloning and expression of the AFP. b) Schematic of the recombinant AFP coating on aluminum surfaces using the oxygen plasma activation technique.

(15 °C, 23 °C, 30 °C, 37 °C), and volume of the culture (5, 200, and 400 mL). To obtain the recombinant AFP from *E. coli* cells, a probe sonicator that disrupted the cell membrane while applying ultrasonic pulses was used. The soluble protein products were purified by dialysis and His-tag affinity chromatography. The purified protein samples were run on SDS-PAGE to visualize the size and expression of the protein.

2.4. Circular Dichroism (CD) Spectroscopy and Thermal Stability Analysis

Secondary structure of the recombinant AFP was evaluated by circular dichroism (CD) spectroscopy measurements by Jasco J-810 CD Spectrophotometer. The process was conducted according to the methodology of Marshall et al.[47] Accordingly, the 60 µg mL^{-1} recombinant AFP sample was dialyzed against 10×10^{-3} M Tris-chloride buffer (pH 8.0) at 4 °C. The dialysis buffer was scanned to establish the baseline CD. Wave scans were obtained between 180 and 260 nm by sampling the data at 1.0 nm and 50 nm min^{-1} scanning rate with three repeating cycles for each data. The results were defined as the mean residue ellipticity (mdeg). The thermal stability analysis was carried out by CD spectroscopy to determine the effect of temperature fluctuations on the secondary structure of the recombinant AFP. For this, several scans were obtained at multiple temperatures (–8°, –4°,0°,4°,8°,10°,20°,30°,40°,50°, and 60°).

2.5. Structure Prediction and Homology Modeling

The amino acid sequence of the *Pseudomonas putida* afpA gene for the AFP was retrieved from the website of the National Centre for Biotechnology Information[48] and was used as a query sequence for structure prediction and homology modeling. The sequence was submitted to NCBI Blast[49] to get the most similar protein with the most similar Crystal structure. The SWISS-MODEL was utilized to obtain the most similar 3D tertiary structure of the recombinant AFP.[50,51]

2.6. Recombinant AFP Immobilization to Aluminum Surfaces

The recombinant AFP was immobilized on oxygen plasma-pretreated aluminum surfaces. Each aluminum surface was treated with oxygen plasma for 1 min to activate functional groups on the surfaces and enhance cross-linking, as shown in Figure 1b.[52] The recombinant AFP immobilization was carried out at zero degrees by spreading the recombinant AFP consisting of 50×10^{-3} M Imidazole solution on the pretreated aluminum surfaces.

2.7. Icing Characterization

A scanning electron microscopy (SEM) (Zeiss Leo Supra 35VP) was employed to characterize the surface structure of the recombinanant AFP coating on aluminum substrates. Contact angle (AC) measurements on the recombinant AFP coated/plain aluminum surfaces were performed to evaluate the wettability of

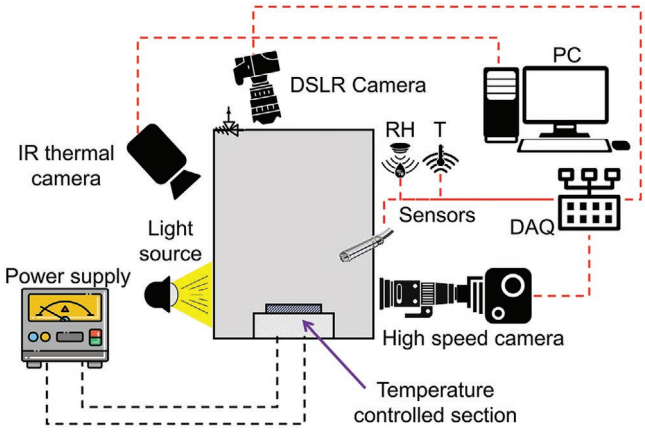

Figure 2. Schematic of the experimental setup.

the developed surfaces. The activity of produced recombinant AFP and the anti-icing activity of the immobilized recombinant AFP were characterized using a lab-made test section. **Figure 2** shows the schematic of the experimental setup. It consists of a closed chamber with relative humidity and temperature regulator, a power supply to regulate the temperature (supercooling temperature) of the tested specimen, temperature and humidity sensors, a data acquisition system (DAQ), and a light source. A high-speed (Phantom v9.1 vision research, 2000 fps), a Digital Single-Lens Reflex (DSLR) (Canon EOS, 30 fps), and an IR thermal camera (FLIR T1020) were used for the observation. The sample was attached to the cold plate of a Peltier cooler (Peltier Module TEG High Temperature) using a thermally conductive adhesive tape (McMaster Carr, 6838A11). The surface subcooling was provided using the Peltier cooler at different temperatures. A liquid cooling loop was used to reduce and maintain the temperature of the hot side of the Peltier device for thermal stability in long icing experiments. The sample surfaces were monitored and measured simultaneously using the thermal camera. The DSLR camera was used to visualize the icing experiments from the top. The humidity and temperature of the chamber were constantly measured and checked with temperature and humidity sensors during the tests (PCE Instruments – PCE-313A, with ±0.1% and ± 0.8 °C precisions in RH and temperature, respectively). The humidity range of the tests was changed from 0.4 to 0.8 to cover a wide range of testing conditions. The temperature of the samples was monitored using an IR thermal camera (FLIR T1020) and a T-type thermocouple. The experiments were repeated for three to five times. The humidity and temperature of the chamber, sample's subcooling, and time were crucial parameters, which were monitored continuously during the experiments. The accuracy of the devices and uncertainties in the experimental parameters are provided in **Table 1**.

Table 1. Accuracy of devices and uncertainty of measurements.

Parameter	Accuracy [%]	Uncertainty [%]
Power supply [V]	0.1	±0.5
Temperature [K]	0.1	±0.1
Data logger [°C]	0.1	±0.1
Multimeter	0.1	±0.01

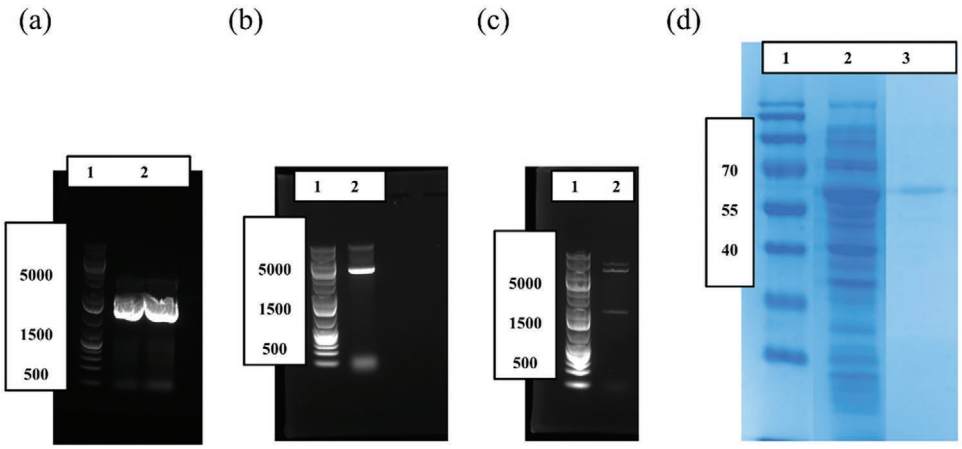

Figure 3. Gel red stained 0.8% agarose gel showing. a) Lane 1, molecular marker (SM1333); Lane 2, PCR Product of pUC-AFP (1.5 kbp). b) Gel red stained 0.8% agarose gel showing; Lane 1, molecular marker (SM1333); Lane 2, pET $_{28}$-AFP. c) Gel red stained 0.8% agarose gel showing; Lane 1, molecular marker (SM1333); Lane 2, double-restricted pET$_{28}$-AFP. d) Sodium dodecyl sulphate-polyacrylamide gel electrophoresis (SDS PAGE) (12%), stained with Coomassie blue, the AFP samples were induced by 0.8×10^{-3} M IPTG. SDS gel shows AFP expression and purification of the recombinant AFP. Lane 1, molecular marker; Lane 2, AFP expression by *E. Coli* Rosetta; Lane 3, partially purified AFP. The size of the recombinant AFP is around 63 kDa.

3. Results

3.1. Construction, Expression, and Optimization of recombinant AFP

The synthetic AFP gene pUC-AFP encoding for the afpA protein in Mryoi et al.[31] was established by the recombinant cloning technology. The recombinant pET$_{28}$-AFP vector was designed as mentioned above. The size of the constructs was confirmed by agarose gel electrophoresis. As shown in **Figure 3**a, the results indicate that the AFP gene was successfully amplified by PCR amplification, where 1.5 kb represents the AFP gene. Besides, the size of the pET$_{28}$-AFP matched with the calculated construct size and was verified by restriction digestion (Figure 3c). The agarose gel electrophoresis confirms that the amplified AFP product was favorably cloned in the pET$_{28}$ expression vector since the size of the pET$_{28}$-AFP matches with the calculated construct size. (pET$_{28}$ band size is 5.4 kb and the recombinant pET$_{28}$-AFP construct is around 6.9 kb, Figure 3b).

Sequencing analysis was performed as mentioned previously. Its results demonstrate that both plasmid constructs, the ligated parts as pET$_{28}$ and AFP, were in the correct order. More information about the sequencing analysis results is provided in Supporting Information 1 and 2.

The SDS PAGE results shown in Figure 3d indicate that produced recombinant AFP has a molecular mass of 63 kDa. The SDS PAGE results lead to optimum parameters to express the recombinant AFP. The optimization experiments allow the production of high recombinant AFP using 0.8×10^{-3} M IPTG induction in 4 h at the incubation temperature of 30 °C.

3.2. CD Spectroscopy and Thermal Analysis

CD spectroscopy analysis was conducted to analyze the recombinant AFP's secondary structure and thermal stability. CD spectrums were collected between –8 °C and 60 °C to determine the effect of temperature change on the recombinant AFP. The

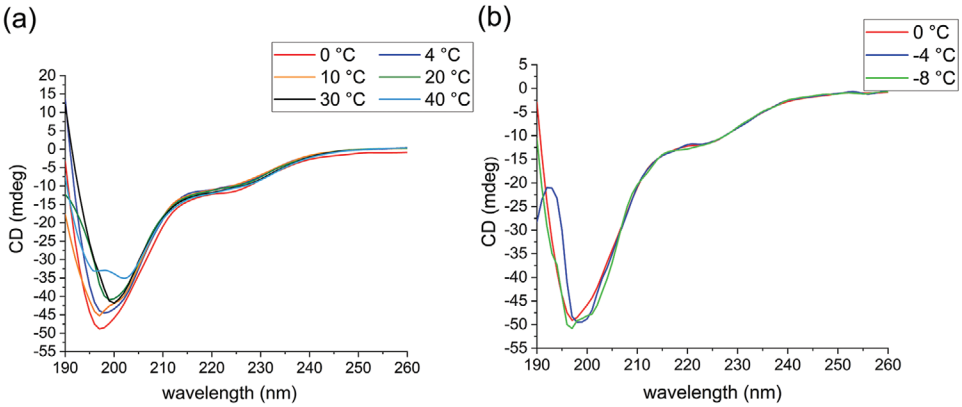

Figure 4. CD spectra of the recombinant AFP, between 190– 260 nm. a) Representation of CD spectrum above 0 °C. 0 °C (red), 4 °C (blue), 10 °C (orange), 20 °C (green), 30 °C (black), and 40 °C (navy blue). b) Representation of CD spectrum below 0 °C. 0 °C (red), –4 °C (blue), –8 °C (green).

CD spectra of the recombinant AFP sample within the range of 190–260 nm display the α-helical spectrum with negative bands at 208 and 222 nm and a positive band at 193 nm.[53] The results show no significant structural change with temperatures up to 40 °C (**Figure 4**a). Besides, the recombinant AFP exhibits structural stability even below zero degrees since it results in the α-helical spectrum until –4 °C where structural distortions could be observed (Figure 4b).

3.3. Structure Prediction and Homology Modeling

Among the proteins whose structure has been determined, AFP from cyanobacterial phycobilisome from *Anabaena sp.* PCC 7120. is found to be most similar, with a homology of 22.7 percent. Therefore, it was used as a template for structure prediction and homology modeling studies, as shown in **Figure 5**. The general properties and amino acid composition of the recombinant AFP are presented in **Tables 2** and **3**, respectively.

3.4. Anti-icing Activity

Figure 6 displays the SEM image of the coated aluminum sample with the recombinant AFP concentration of 60 µg mL^{-1}. As can be seen, the coating has a smooth profile with an average roughness value of 1.7 µm (Figure 6). SEM might induce radiation damage on the biological samples,[55] the "vein-like" structures could be partially denatured proteins due to harsh conditions during SEM analysis. While exposure to room temperature gradually reduces the life span of the AFPs, the electron beams break down the structure of the protein.

Figure 7 shows the CA results of the recombinant AFP coated aluminum and plain aluminum surfaces. Accordingly, both of the surfaces exhibit hydrophilic nature. However, a slight increase in the wettability of the recombinant AFP coated sample can be noticed.

Anti-icing performances of the recombinant AFP-immobilized surfaces were investigated and compared to those of the reference samples (plain) at sub-zero temperatures. **Figure 8** shows the icing on the plain surface and the anti-icing activity of the AFP-coated surface with the AFP concentration of 60 µg mL^{-1} at the surface temperature of –4 °C. Significant ice formation can be observed on the bare substrates at early stages, and ice completely covers the surface in less than 10 s. However, although ice formation occurs on a small area on the coated samples, ice growth is hampered due to the presence of AFPs.

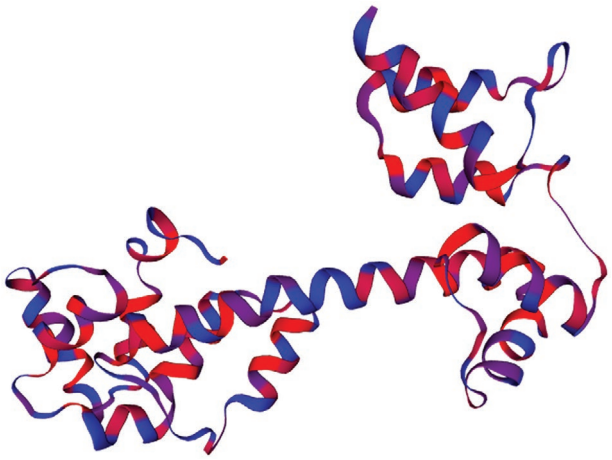

Figure 5. Predicted structure of the recombinant AFP with 22.7% similarity of Phycobiliprotein ApcE Cryo-EM structure of cyanobacterial phycobilisome from Anabaena sp. PCC 7120.[54]

Table 2. General Properties of AFP.[49]

Recombinant AFP	
Number of amino acids	473
Molecular weight	47 316.12 Da
Theoretical pI	3.67
Total number of negatively charged residues (Asp + Glu)	61
Total number of positively charged residues (Arg + Lys)	10
Charge	Negative

4. Discussion

In the current study, the synthetic AFP gene (pUC-AFP) having the same amino acid sequence as the original afpA in Mryoi et al.[44] was established by the recombinant cloning technology. The original microorganism is the plant growth-promoting rhizobacterium *P. Putida* GR12-2, isolated from a soil sample from the Canadian High Arctic. The afpA was expressed by *P. putida* GR12-2 inside a growth medium at a cold temperature range. The recombinant AFP was expressed using *E. coli* strain Rosetta (DE3) cells by the IPTG induction. The SDS PAGE results exhibited in Figure 3 indicate that produced recombinant AFP has a molecular mass of 63 kDa, whereas the original afpA has a size of 72 kDa, which is even higher than the predicted size, 47.3 kDa (Figure 3d). The mass difference could be attributed to the posttranslational modifications (PTMs). PTMs are chemical modifications affecting protein stability, net charge, binding properties, conformation, and localization.[56,57]

Table 3. Amino acid composition of recombinant AFP.[49]

Ala (A) 82	17.3%	Lys (K) 3	0.6%
Arg (R) 1.5%	1.5%	Met (M) 1	0.2%
Asn (N) 34	7.2%	Phe (F) 14	3.0%
Asp (D) 38	8.0%	Pro (P) 8	1.7%
Cys (C) 0	0.0%	Ser (S) 39	8.2%
Gln (Q) 16	3.4%	Thr (T) 42	8.9%
Glu (E) 23	4.9%	Trp (W) 4	0.8%
Gly (G) 53	11.2%	Tyr (Y) 8	1.7%
His (H) 4	0.8%	Val (V) 35	7.4%
Ile (I) 30	6.3%	Pyl (O) 0	0.0%
Leu (L) 32	6.8%	Sec (U) 0	0.0%

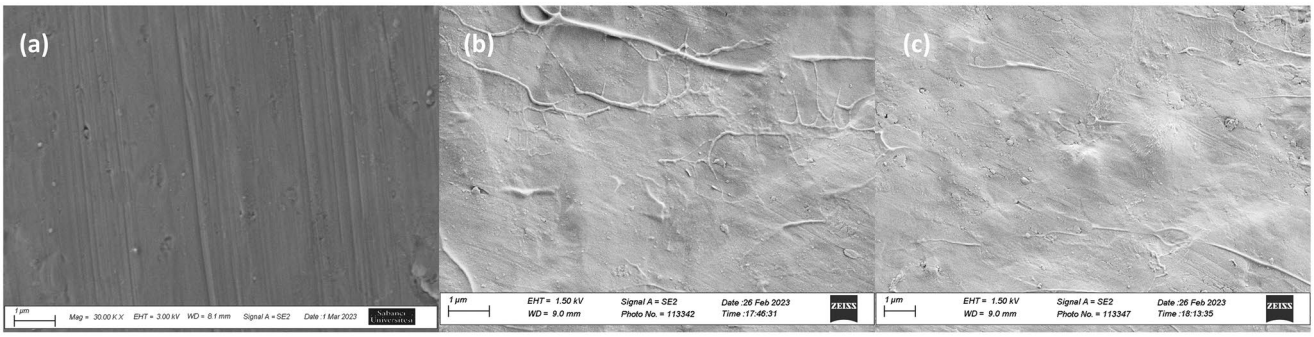

Figure 6. a) SEM image of the plain aluminum surface and b,c) SEM images of the recombinant AFP coated aluminum surface.

Several modifications such as proteolytic cleavage, phosphorylation, glycosylation, methylation, acetylation, and lipidation raise PTMs in proteins and consequently alter protein characteristics such as molecular weight.[58,59] The functionality of AFPs is diversified by their ice-binding site (IBS), which alters binding through ice crystal planes. The diversity in amino acid sequence and structure folding of AFPs affects the ice-binding affinity.[60] However, residual variations in the AFPs might have a direct relationship with the antifreeze activity of the AFPs.[61] It is suggested that Threonine repeating units play a significant role in conformational change as well as ice-binding properties of various AFPs rendered by methyl and hydroxyl functional groups.[62] As indicated in Table 3, the most repeated residues in the amino acid sequence are Ala (17.3%), Gly (11.2%), Thr (8.9%), Ser (8.2%), Asp (8%), and Asn (7.2%). The Alanine (Ala) and Threonine (Thr) residues are essential residues in the IBS of the recombinant AFP. **Figure 9** shows the position of the hydrophobic region of a-helix.[22] The polypeptides present the best IRI activity among arginine polypeptides and glutamic acid polypeptides.[63] Besides, Glycine (Gly) amino acids have an essential role in the formation of IBS due to conformationally flexible structure.[64] Cysteine (Cys), Serine (Ser), Tryptophan (Trp), Gly, Asparagine (Asn), and Thr are the particular residues of AFPs.[65,66] In addition, the insignificant number of hydrophobic residues such as Leucine (Leu), Valine (Val), and Isoleucine (Ile), which are particularly notable in highly stable proteins, is perhaps one of the main reasons for the low stability of this protein at higher temperatures.[67]

Repeating TxT sequences (T is Threonine and x is a non-conserved amino acid) have strong binding efficiency to the ice by anchored clathrate (AC) motifs.[68] The clathrate-like water molecules are formed around the methyl groups of the Thr residues by water molecules in the AC motifs and the bound hydroxyl group of the proteins. The hydrophobicity of the AFPs is another key parameter. The IBSs of the AFPs are hydrophobic, affecting water molecules' ordering during ice formation.[69,70] The recombinant AFP could be considered an effective AFP due to the abundance of Ala, Gly, and Thr residues, having 4 TxT repeated sequences and hydrophobic characteristics in the whole sequence, demonstrating the functional IBS of the recombinant AFP (**Figure 10**).

3D structure prediction is based on models already determined through the X-Ray crystallization method. The most homologous protein to the recombinant AFP has a maximum of 22.7% homology. Based on this homology, we modeled our protein using the Expasy database to have knowledge about the kinetics mechanism and configurations of active sites of the recombinant AFP. Together with CD spectrum results, the secondary structure prediction of the recombinant AFP protein will help us in one step closer understanding of the kinetics and mechanism of the recombinant AFP.

The amino acid analysis of the AFP protein leads to the highest amount of alanine residues (17.3%) which is generally the reason for forming a coiled-coil structure. The CD spectra of AFP at various temperatures follow the same pattern shown in the coiled–coil secondary structure. These types of α-helices are situated in the interior part of the protein chain.[71] Moreover, as the alanine residues bury more apolar regions during folding and have lower backbone entropy, they stabilize the helical conformation more consistently than glycine.[72] Based

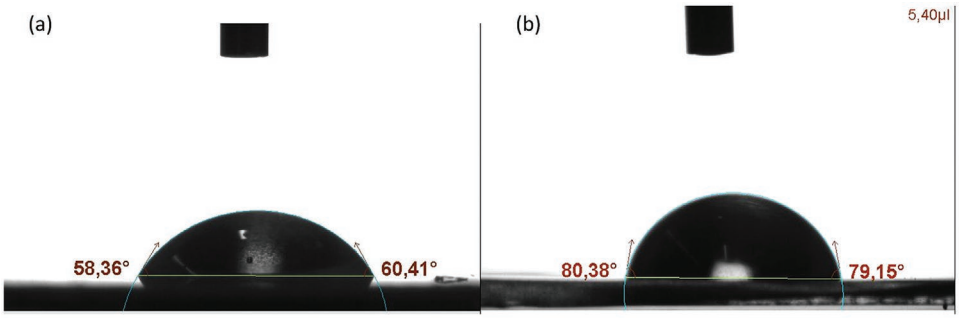

Figure 7. CA results of a) recombinant AFP coated aluminum surfaces. b) Plain aluminum surface.

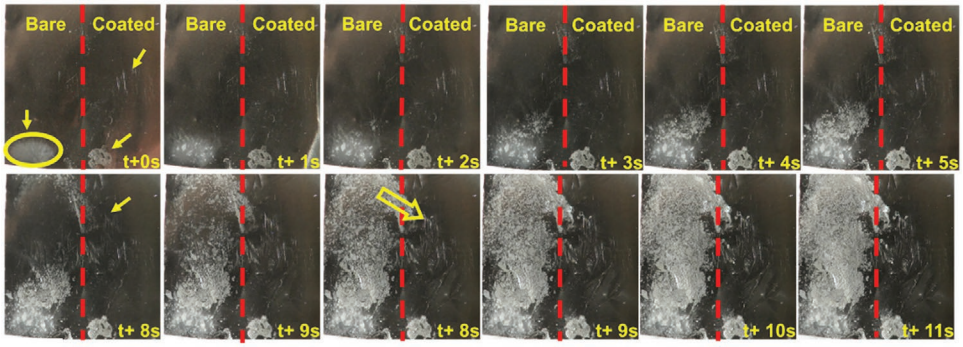

Figure 8. The icing behaviour on recombinant AFP coated and plain aluminum surfaces.

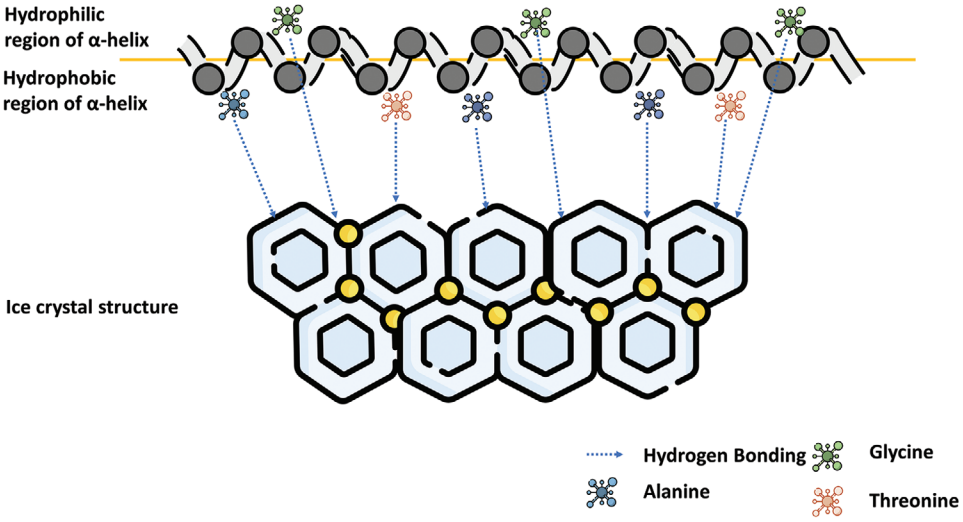

Figure 9. Schematic representation of ice-binding of threonine (orange), glycine (green), and alanine (blue) residues to the ice crystals by hydrogen bonding.

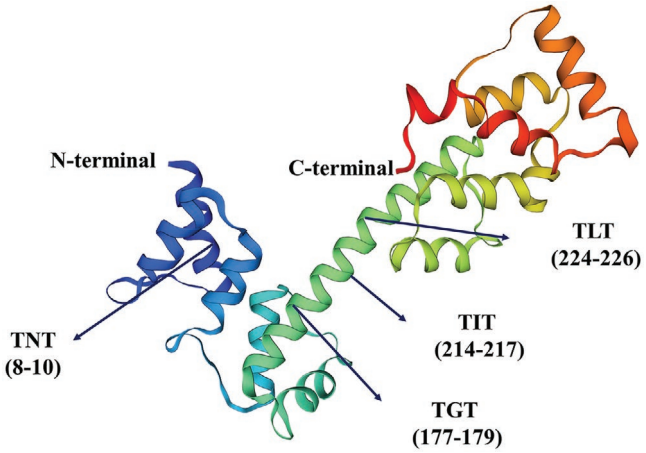

Figure 10. The predicted 3D structure of the AFP shows TxT repeating units.[54]

on our observations, the AFP protein maintains the structure of a coiled-coil structure at lower temperatures (←8 °C). The flexibility is further minimized with a similar pattern with a slightly negative peak at ~200 nm.

AFPs hampers the ice formation in a noncolligative manner by ceasing the ice crystal growth through a concentration-dependent temperature range explained by the adsorption-inhibition hypothesis.[73] Herein, a critical concentration value, which decreases in function of temperature, must be exceeded by the surface concentration of adsorbed AFP molecules to inhibit ice crystal growth. AFPs can present IRI activity even at submicromolar concentrations, while TH activity requires millimolar concentrations.[25,74] Therefore, IRI is assumed to be the primary function of AFPs secreting from several cold-adapted organisms.[75] Besides, it was reported that the TH value of fungus-originated AFP increases with protein concentration.[60] Although both TH and IRI activity alter the ice adsorption of AFPs, there is no definite correlation between IRI and TH.[23]

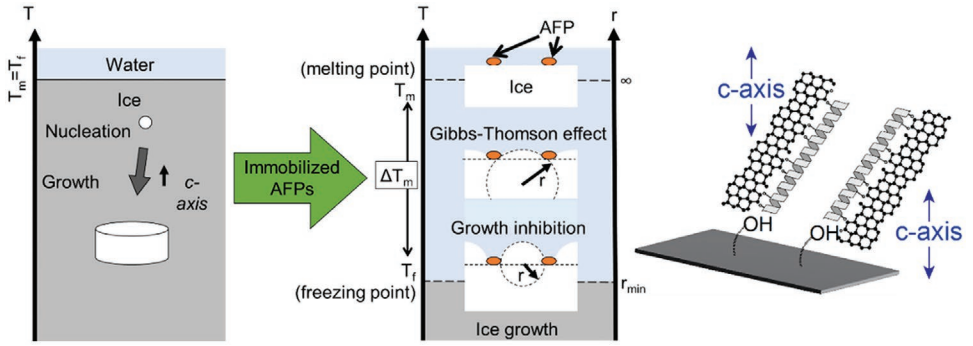

Figure 11. Schematic of ice growth in water and Gibbs–Thomson model for ice growth inhabitation by AFP (left) and immobilized AFPs on aluminum surfaces (right).

Thus, we could assume that the recombinant-AFP indicates IRI activity due to micromolar concentrations.

The ability of the recombinant AFP to hinder ice crystal growth is attributed to the binding of AFPs to specific interfaces on ice crystals. When AFP experiences irreversibly binding to an interface of a growing ice crystal, the interface around the AFP becomes curvy (**Figure 11**). As a result, the melting temperature (T_m) at the curved interface becomes locally lower than the T_m of bulk ice because of the Gibbs–Thomson effect. Assuming the growth of a spherical ice crystal with a radius r around AFPs at an interface of an ice crystal, the thermal hysteresis (TH – ΔT_m) caused by the Gibbs–Thomson effect is given as:[76]

$$\Delta T_m = \frac{2\sigma_{sl} T_m}{r \Delta H_f \rho_s} \quad (1)$$

Here, σ_{sl} is the surface tension between solid and liquid phases,ΔH_f is the heat of fusion, ρ_s is the density of the solid phase, and r is the radius of the ice crystal. ΔT_m increases as r decreases and reaches a maximum when r decreases to half the distance between two AFP molecules bound to the interface (r_{min}). In this case, the shape of the grown ice crystal corresponds to a hemisphere. It can be assumed that r_{min} is inversely proportional to the AFP concentration ($\times 10^{-3}$ M). Thus, the maximum of ΔT_m, which corresponds to ΔT_{mf}, increases with concentration. Consequently, the model based on the Gibbs–Thomson effect qualitatively explains why the binding of the recombinant AFP inhibits ice growth to an ice interface.

Unlike the available superhydrophobic surfaces/coatings that suggest water repellency as the main reason responsible for anti-icing, the mechanism responsible for the anti-icing of activity of the AFP-coated substrate is related to the Gibbs–Thomson effect. CA measurements (Figure 7) show that the AFP-coated surfaces are hydrophilic. The molecular level of hydrophobicity (hydrophobic parts of the α-helix of the protein) and low concentration of AFPs (60 µg mL^{-1}) could be the main reasons for the hydrophilicity of the coated substrates.

5. Conclusion

This study presents the production of AFP using the recombinant technology, followed by its novel immobilization on aluminum surfaces and further demonstration of anti-icing activity. The major goal is to propose environmentally friendly and scalable coating and to show its applicability to relevant industries such as refrigeration systems. The recombinant technology enables large-scale protein production of the AFP for industrial applications via surface immobilization methods. The application of oxygen plasma allows the activation of surface functional groups and is suitable for different shapes and geometries while increasing the coating stability. In the current study, produced recombinant AFP was coated on aluminum surfaces with oxygen plasma pretreatment, and the activity of AFP-immobilized surfaces was tested under different conditions. The recombinant AFP-coated substrates exhibit a significant anti-icing performance compared to uncoated surfaces in terms of ice growth due to the Gibbs–Thomson effect. Consequently, this study offers a new perspective for biotechnological implementation of AFPs to ensure energy-saving and efficiency with an environmentally friendly aspect. The coating proposed in this study can be used as a futuristic biological coating for the next generation of appliances and heat exchangers with applications in space heating and cooling, refrigeration, air conditioning, as well as a scalable and low-cost biological heat transfer coating.

Supporting Information

Supporting Information is available from the Wiley Online Library or from the author.

Acknowledgements

This study was conducted under the scope of MEraNet Project "Biotechnological Antifreeze Coating-BioAFC" and supported by TÜBİTAK (The Scientific and Technological Research Council of Turkey) Multiple Cooperation Support Programs 1071 Grant No. 121N564.

Conflict of Interest

The authors declare no conflict of interest.

Author Contributions

Z.M. worked on methodology, investigation, data curation, and also wrote the original draft, reviewed, and edited the work. G.G. worked on conceptualization, methodology, investigation, data curation, and wrote the original draft, reviewed and edited the work; supervised the work and worked on project administration. S.S. worked on methodology, investigated the work, wrote, reviewed, and edited the work. R.R. worked on project administration, funding, and drafted the work. V.S. worked on project administration, funding and drafted the work. A.J. worked on project administration, funding, and drafted the work. A.K. worked on conceptualization, methodology, investigation, resources, and wrote the original draft, reviewed and edited the work; supervised the work and worked on project administration. A.S. worked on conceptualization, methodology, investigation, resources, data curation, and wrote the original draft, reviewed, and edited the work; supervised the work and worked on project administration.

Data Availability Statement

The data that support the findings of this study are available from the corresponding author upon reasonable request.

Keywords

antifreeze activity, antifreeze coating, antifreeze proteins, ice binding proteins, industrial applications, metallic surfaces

Received: January 8, 2023
Revised: March 3, 2023
Published online:

[1] W. Huang, J. Huang, Z. Guo, W. Liu, *Adv. Colloid Interface Sci.* **2022**, *304*, 102658.
[2] S. Jiang, Y. Diao, H. Yang, *Adv. Colloid Interface Sci.* **2022**, *308*, 102756.
[3] G. V. Vaganov, V. V. Vaganov, I. L. Radchenko, I. A. Ilyina, *IOP Conf. Ser.: Earth Environ. Sci.* **2020**, *539*, 012038.
[4] Z. He, H. Xie, M. I. Jamil, T. Li, Q. Zhang, *Adv. Mater. Interfaces* **2022**, *9*, 2200275.
[5] Z. He, M. I. Jamil, T. Li, Q. Zhang, *Langmuir* **2022**, *38*, 18.
[6] X. Li, Y. Zhao, H. Li, X. Yuan, *Appl. Surf. Sci.* **2014**, *316*, 222.
[7] Z. Wang, Y. Zhu, X. Liu, Z. Zhao, J. Chen, X. Jing, H. Chen, *Chem. Eng. J.* **2021**, *422*, 130110.
[8] L.-B.o Zhang, H.-X. Zhang, Z.-J. Liu, X.-Y.u Jiang, S. Agathopoulos, Z. Deng, H.-Y.u Gao, L.i Zhang, H.-P. Lu, L.-J. Deng, L.-J. Yin, *J. Colloid Interface Sci.* **2023**, *630*, 1.
[9] Y. Liu, Y. Shao, Y. Wang, J. Wang, *Colloids Surf. A* **2022**, *648*, 129335.
[10] D. Zeng, Y. Li, D. Huan, H. Liu, H. Luo, Y. Cui, C. Zhu, J. Wang, *Colloids Surf. A* **2021**, *628*, 127377.
[11] Y. Gwak, J. i-I. n Park, M. Kim, H. S. Kim, M. J. Kwon, S. J. Oh, Y.-P. Kim, E. Jin, *Sci. Rep.* **2015**, *5*, 12019.
[12] O. Carrión, L. Delgado, E. Mercade, *Carbohydr. Polym.* **2015**, *117*, 1028.
[13] D. Brisson, M.-C. Vohl, J. St-Pierre, T. J. Hudson, D. Gaudet, *BioEssays* **2001**, *23*, 534.
[14] X.u Chen, J. Wu, L. Li, S. Wang, *J. Agric. Food Chem.* **2019**, *67*, 1918.
[15] G. A. MacDonald, T. C. Lanier, *Quality in Frozen Food*, (Eds: M.C. Erickson, Y.-C. Hung), Springer US, Boston, MA **1997**, pp. 197–232.
[16] S. G. Sutariya, V. Sunkesula, *Innovative Food Processing Technologies*, (Eds: K. Knoerzer, K. Muthukumarappan), Elsevier, Oxford **2021**, pp. 36–63.
[17] A. Baskaran, M. Kaari, G. Venugopal, R. Manikkam, J. Joseph, P. V. Bhaskar, *Int. J. Biol. Macromol.* **2021**, *189*, 292.
[18] J. G. Duman, *J. Exp. Biol.* **2015**, *218*, 1846.
[19] L. L. C. Olijve, K. Meister, A. L. Devries, J. G. Duman, S. Guo, H. J. Bakker, I. K. Voets, *Proc. Natl. Acad. Sci. USA* **2016**, *113*, 3740.
[20] A. Eskandari, T. C. Leow, M. B. A. Rahman, S. N. Oslan, *Biomolecules* **2020**, *10*, 1649.
[21] P. L. Davies, B. D. Sykes, *Curr. Opin. Struct. Biol.* **1997**, *7*, 828.
[22] G. Gharib, S. Saeidiharzand, A. K. Sadaghiani, A. Koşar, *Front. Bioeng. Biotechnol.* **2022**, *9*, 770588.
[23] H. Xiang, X. Yang, L. Ke, Y. Hu, *Int. J. Biol. Macromol.* **2020**, *153*, 661.
[24] A. T. Rahman, T. Arai, A. Yamauchi, A.i Miura, H. Kondo, Y. Ohyama, S. Tsuda, *Sci. Rep.* **2019**, *9*, 2212.
[25] L. L. C. Olijve, K. Meister, A. L. DeVries, I. K. Voets, *Proc. Natl. Acad. Sci. USA* **2016**, *113*, 3740.
[26] G. Gharib, S. Saeidiharzand, A. K. Sadaghiani, A. Koşar, *Front. Bioeng. Biotechnol.* **2022**, *9*, 1530.
[27] M. G. A. Da Cruz, T. M. Budnyak, B. V. M. Rodrigues, S. Budnyk, A. Slabon, *Green Chem. Lett. Rev.* **2021**, *14*, 358.
[28] Q. Zeng, S. Xue, J. Li, W. Jiang, Y. Ding, L. Shen, *Prog. Org. Coat.* **2022**, *171*, 107040.
[29] A. D. Kashin, M. B. Sedelnikova, V. V. Chebodaeva, P. V. Uvarkin, N. A. Luginin, E. S. Dvilis, O. V. Kazmina, Y.u.P. Sharkeev, I. A. Khlusov, A. A. Miller, O. V. Bakina, *Ceram. Int.* **2022**, *48*, 28059.
[30] Y. Fang, L. Chen, J. Wu, X. Liu, *Ind. Crops Prod.* **2022**, *187*, 115456.
[31] I. Rodrigues, T. M. Mata, A. A. Martins, *J. Cleaner Prod.* **2022**, *367*, 133011.
[32] S. Jafarzadeh, A. Mohammadi Nafchi, A. Salehabadi, N. Oladzad-Abbasabadi, S. M. Jafari, *Adv. Colloid Interface Sci.* **2021**, *291*, 102405.
[33] H. Du, F. Liu, H. Wang, *J. Colloid Interface Sci.* **2022**, *616*, 720.
[34] S. Niazi, A. K. Sadaghiani, G. Gharib, V. O. Kaya, S. Çelik, Ö. Kutlu, A. Koşar, *Energy* **2021**, *222*, 119959.
[35] A. Duman, S. Niazi, G. Gharib, A. K. Sadaghiani, A. Koşar, *Int. J. Thermofluids* **2022**, *15*, 100170.
[36] H. Qi, C. Zhang, H. Guo, W. Zheng, J. Yang, X. Zhou, L. Zhang, *ACS Appl. Mater. Interfaces* **2019**, *11*, 24504.
[37] F. Song, Q. Zhao, T. Zhu, C. Bo, M. Zhang, L. Hu, X. Zhu, P. Jia, Y. Zhou, *Mater. Des.* **2022**, *221*, 110925.
[38] A. P. Esser-Kahn, V. Trang, M. B. Francis, *J. Am. Chem. Soc.* **2010**, *132*, 13264.
[39] J. K. Kaushik, R. Bhat, *J. Biol. Chem.* **2003**, *278*, 26458.
[40] K. Koshio, K. Arai, T. Waku, P. W. Wilson, Y. Hagiwara, *PLoS One* **2018**, *13*, e0204686.
[41] Y. Jeong, S. Jeong, Y. K. Nam, S. M. Kang, *Bull. Korean Chem. Soc.* **2018**, *39*, 559.
[42] Z. Chen, C.-Y. Huang, M. Zhao, W. Yan, C.-W. Chien, M. Chen, H. Yang, H. Machiyama, S. Lin, *J. Asian Earth Sci.* **2011**, *40*, 363.
[43] D. Brough, H. Jouhara, *Int. J. Thermofluids* **2020**, *1–2*, 100007.
[44] N. Muryoi, M. Sato, S. Kaneko, H. Kawahara, H. Obata, M. W. F. Yaish, M. Griffith, B. R. Glick, *J. Bacteriol.* **2004**, *186*, 5661.
[45] J. Sambrook, E. F. Fritsch, T. Maniatis, *Molecular Cloning: A Laboratory Manual*, Cold Spring Harbor Laboratory Press, NY, USA **1989**.
[46] R. Osborne, *WO2017037656A1*, **2015**.
[47] C. B. Marshall, A. Chakrabartty, P. L. Davies, *J. Biol. Chem.* **2005**, *280*, 17920.
[48] National Center for Biotechnology Information, https://www.ncbi.nlm.nih.gov/nuccore/AJ784158
[49] National Center for Biotechnology Information, http://blast.ncbi.nlm.nih.gov/Blast.cgi

[50] A. Waterhouse, M. Bertoni, S. Bienert, G. Studer, G. Tauriello, R. Gumienny, F. T. Heer, T. A. P. De Beer, C. Rempfer, L. Bordoli, R. Lepore, T. Schwede, *Nucleic Acids Res.* **2018**, *46*, W296.
[51] N. Guex, M. C. Peitsch, T. Schwede, *Electrophoresis* **2009**, *30*, S162.
[52] N. De Geyter, R. Morent, *Biomaterials for Bone Regeneration*, (Eds: P. Dubruel, S. Van Vlierberghe), Woodhead Publishing, Sawston, UK **2014**, pp. 202–224.
[53] N. J. Greenfield, *Nat. Protoc.* **2006**, *1*, 2876.
[54] SWISS-MODEL, https://swissmodel.expasy.org/.
[55] T. Ogura, *PLoS One* **2012**, *7*, e46904.
[56] A. Hashiguchi, S. Komatsu, *Methods in Enzymology*, (Ed: A.K. Shukla), Academic Press, Cambridge, MA, USA **2017**, pp. 97–113.
[57] B. Macek, K. Forchhammer, J. Hardouin, E. Weber-Ban, C. Grangeasse, I. Mijakovic, *Nat. Rev. Microbiol.* **2019**, *17*, 651.
[58] S. Ramazi, J. Zahiri, *Database* **2021**, *2021*, baab012.
[59] M. R. Larsen, M. B. Trelle, T. E. Thingholm, O. N. Jensen, *Biotechniques* **2006**, *40*, 790.
[60] N. M.-M. U. Khan, T. Arai, S. Tsuda, H. Kondo, *Sci. Rep.* **2021**, *11*, 5971.
[61] C. Wang, S. Pakhomova, M. E. Newcomer, B. C. Christner, B.-H. Luo, *PLoS One* **2017**, *12*, e0187169.
[62] W. Zhang, R. A. Laursen, *J. Biol. Chem.* **1998**, *273*, 34806.
[63] E. A. Delesky, L. Garcia, A. Lobo, J. Wallat, G. Miyake, W. Srubar, *ChemRxiv* **2021**.
[64] S. Sun, H. Ding, D. Wang, S. Han, *Front. Bioeng. Biotechnol.* **2020**, *8*, 244.
[65] R. Pratiwi, A. A. Malik, N. Schaduangrat, V. Prachayasittikul, J. E. S. Wikberg, C. Nantasenamat, W. Shoombuatong, *J. Chem.* **2017**, *2017*, 9861752.
[66] R. Miyata, Y. Moriwaki, T. Terada, K. Shimizu, *Heliyon* **2021**, *7*, e07953.
[67] G. Gharib, N. Rashid, Q. Bashir, Q.-.T. A. A. Gardner, M. Akhtar, T. Imanaka, *Extremophiles* **2016**, *20*, 57.
[68] A. Hudait, Y. Qiu, N. Odendahl, V. Molinero, *J. Am. Chem. Soc.* **2019**, *141*, 7887.
[69] Y. Hanada, Y. Nishimiya, A.i Miura, S. Tsuda, H. Kondo, *FEBS J* **2014**, *281*, 3576.
[70] P. L. Davies, *Trends Biochem. Sci.* **2014**, *39*, 548.
[71] T. Kameda, *Polym. J.* **2012**, *44*, 876.
[72] J. López-Llano, L. A. Campos, J. Sancho, *Proteins* **2006**, *64*, 769.
[73] L. Chapsky, B. Rubinsky, *FEBS Lett.* **1997**, *412*, 241.
[74] S. O. Yu, A. Brown, A. J. Middleton, M. M. Tomczak, V. K. Walker, P. L. Davies, *Cryobiology* **2010**, *61*, 327.
[75] T. Collins, R. Margesin, *Appl. Microbiol. Biotechnol.* **2019**, *103*, 2857.
[76] J. Gerhäuser, V. Gaukel, *Langmuir* **2021**, *37*, 11716.